DEVELOPMENTAL DYNAMICS 246:812–826, 2017
DOI: 10.1002/DVDY.24496

RESEARCH ARTICLE

Gastrulation in an Annual Killifish: Molecular and Cellular Events During Germ Layer Formation in *Austrolebias*

Luisa Pereiro,[1] Felix Loosli,[2] Juan Fernández,[3] Steffen Härtel,[1,4,7] Joachim Wittbrodt,[5] and Miguel L. Concha [1,4,6]*

[1]Anatomy and Developmental Biology, Institute of Biomedical Sciences, Faculty of Medicine, Universidad de Chile, Santiago, Chile
[2]Karlsruhe Institute of Technology, Institute of Toxicology and Genetics, Karlsruhe, Germany
[3]Department of Biology, Faculty of Sciences, Universidad de Chile, Santiago, Chile
[4]Biomedical Neuroscience Institute, Santiago, Chile
[5]Center for Organismal Studies, Heidelberg University, Heidelberg, Germany
[6]Center for Geroscience, Brain Health and Metabolism, Santiago, Chile
[7]National Center for Health Information Systems CENS, Santiago, Chile

Background: Comparative studies beyond the traditional model organisms have been instrumental in enhancing our understanding of the conserved and derived features of gastrulation, a fundamental process in which the germ layers are specified and shaped to form the body axis. Here, we analyzed gastrulation in a vertebrate group with an extreme mode of early development, the annual killifish. **Results:** Gastrulation in annual killifish of the genus *Austrolebias* takes place after the initially dispersed deep blastomeres congregate to form the so-called reaggregate. Cells from the early reaggregate do not appear to form part of any recognizable axial embryonic structure and are possibly extraembryonic. In contrast, later reaggregate cells become engaged in morphogenetic transformations indicative of a process of gastrulation and axis formation. The expression of *brachyury* and *goosecoid* suggests that gastrulation takes place in a compressed blastopore-like structure with an organizer region displaced to one end. No collective cell internalization proper of blastopore architecture is observed, though, and it appears that gastrulation primarily involves the reorganization of individual cells. **Conclusions:** The unique mode of gastrulation in annual killifish demonstrates that a process so ancient and fundamental to ontogenesis can have striking morphogenetic variations nonpredicted from the sole examination of model species. *Developmental Dynamics 246:812–826, 2017*. © 2017 Wiley Periodicals, Inc.

Key words: Gastrulation; axis formation; *brachyury*; *goosecoid*; annual killifish; *Austrolebias*

Submitted 26 December 2016; First Decision 27 January 2017; Accepted 28 January 2017; Published online 1 March 2017

Introduction

Among vertebrates, the passage from the fertilized egg to a polarized embryonic axis is marked by the morphogenetic reorganization of cells called gastrulation, a process that can adopt many forms depending on the animal group. The diversity of life cycles, reproductive strategies, and physical, temporal, and environmental constraints can clearly impinge upon the way the early embryonic cells move and interact with one another to create form. Despite the variations in the course of action available, conserved and recognizably homologous events can be distinguished: Epiboly, emboly/internalization, convergence, and extension are cell movements shared by all vertebrates, and they allow the germ layers and essential body plan to be established (Keller et al., 2003). Also, an organizer region that initiates the movements that build the head mesendoderm is present in the dorsal blastopore lip of amphibians, the embryonic shield of teleosts, the early Hensen's node of birds, and the anterior primitive streak of mammals (Spemann and Mangold, 1924; Solnica-Krezel and Sepich, 2012).

Cell internalization is the hallmark of gastrulation and it can take place through the formation of a ring or blastopore, as in fishes and amphibians, or a of streak or furrow, as in most amniotes (Keller et al., 2003; Tam and Loebel, 2007; Solnica-Krezel and Sepich, 2012). Despite the overall conservation of these two modes of gastrulation, there is considerable variation among species. For instance, internalization occurs through a circular cleft (blastopore) located between the animal and vegetal hemispheres in *Xenopus* and Zebrafish (Kane and Adams, 2002; Keller et al., 2003), at the edges of an embryonic disk in the frog *Gastrotheca riobambae* (Elinson and del Pino, 2011), and in the posterior margin of the blastoderm in the spotted dogfish *Scyliorhinus canicula* (Coolen et al., 2007). In amniotes, a structure that shifts from ring-like to horseshoe shape is the site of internalization in the turtle *Emys orbiculares* (Coolen et al., 2008), while in chick internalization takes place through an elongated primitive streak at the center of a cellular disk

Additional supporting information may be found in the online version of this article

*Correspondence to: Miguel L. Concha, Anatomy and Developmental Biology, Institute of Biomedical Sciences, Faculty of Medicine, Universidad de Chile, PO Box 70031, Santiago, Chile. Email: mconcha@med.uchile.cl

Article is online at: http://onlinelibrary.wiley.com/doi/10.1002/dvdy.24496/abstract

(Chuai and Weijer, 2008). Variation in gastrulation is also present in the cellular mechanisms deployed for internalization, which can involve epithelial bending or involution (e.g., *Xenopus*), concerted collective cell ingression (e.g., Zebrafish), single-cell delamination (e.g., mouse), or a combination of these processes (Keller et al., 2003; Solnica-Krezel and Sepich, 2012; Williams et al., 2012). Finally, an additional source of variation in gastrulation is the presence of extraembryonic tissues, which in some species provide signals that pattern the site and mode of gastrulation (Ho et al., 1999; Stern and Downs, 2012; Godard and Mazan, 2013).

The teleosts are a monophyletic group of bony fish belonging to the subclass *Actinopterygii* (Nelson, 1984). Though they are by far the most diverse and plentiful in the number of species among the vertebrates, only a few have been examined for the process of gastrulation. The consensus among the modest available selection of models is that after a meroblastic cleavage and blastulation, gastrulation takes place while the blastoderm is expanding over the yolk during the movement of epiboly. In fact, in the most intensely studied fish embryo, the Zebrafish, by the end of epiboly, a tail bud, notochord, and numerous somites are formed and plainly visible (Kimmel et al., 1995). This generalization exists despite the elegant work of John P. Wourms (1935–2013), a comparative developmental biologist who studied, among many species, the annual killifish of the order *Cyprinodontiformes*. Distributed in both the Old World and New World, annual killifish display the remarkable ability to resist a dry season as embryos by undergoing diapauses, reversible metabolic shutdowns that temporarily arrest development. But there is another salient feature of embryogenesis in annual killifish that caught the attention of Wourms: a complete dispersal and subsequent reaggregation of the deep blastomeres before the formation of the embryonic axis, which arises from a discoidal-shaped congregation of cells (Wourms, 1972b; Wourms, 1972c). Blastomeres are few and spread vegetally over the yolk, not as a sheet, but as individual cells with no sign of a germ ring, blastopore, or shield, until epiboly is complete. This dispersal stage can then span hours or months, depending on the occurrence or not of the first of the facultative diapauses (Diapause I) (Wourms, 1972a). Cells then reaggregate at a point on the yolk surface, breaking radial symmetry, to form a mass from which an axis emerges (Wourms, 1972c). In other words, gastrulation is completely uncoupled from epiboly, yet we still end up with a typical teleost morphology once the germ layers are specified. Wourms (Wourms, 1972c) proposed that the reaggregate could be functionally and developmentally homologous to the embryonic shield of other teleost embryos. However, he was aware that it was critical to examine the precise cellular movements that occurred within the reaggregate to confidently make this claim.

In this work, we aimed to provide a more detailed description of the molecular and cellular events occurring during gastrulation in an annual killifish. We analyzed species of the South American genus *Austrolebias* (Costa, 1998), a clade distributed among the Atlantic coastal lowlands of Argentina, Brazil, and Uruguay. Its slow development, the large size of the fertilized egg, and the absence of genetic tools and molecular markers made this analysis challenging. We were able to overcome some of these hurdles by establishing light and confocal microscopy mounting methods, injection of mRNA-encoding fluorescent proteins or photoconvertible lineage tracers, cloning of gastrulation relevant genes, and in situ hybridization. We found that the early reaggregate of *Austrolebias* does not form part of any recognizable axial embryonic structure and thus appears extraembryonic. In contrast, the later reaggregate becomes progressively engaged in morphogenetic transformations, suggestive of a process of gastrulation and axis formation. The analysis of molecular markers suggests the formation of a compressed blastopore-like structure within the reaggregate, although no pattern of collective cell internalization proper of a blastopore can be recognized. Instead, centripetal movements and events of single-cell reorganization appear to shape the cellular reaggregate during gastrulation. Our work sets the stage for further progress in understanding the unique mode of gastrulation in annual killifish, which differs from that of other non-annual teleosts described to date.

Results

As observed in other teleost species, the first stages of development in *Austrolebias charrua* and *A. bellottii* involve cleavage and blastulation at the animal region of the egg, as well as the segregation of three cell populations: an external enveloping cell layer (EVL) of squamous epithelial cells, an internal yolk syncytial layer (YSL) consisting of a syncytium whose nuclei lie within the yolk, and a deep layer of blastomeres (deep cell layer; DCL) that locates between the EVL and YSL and contains the precursors of the embryo proper. When epiboly begins, *Austrolebias* embryos follow a developmental pattern that is characteristic of other annual killifish species (Wourms, 1972c) and differs from the typical pattern of teleost development (Kimmel et al., 1995). Prospective embryonic cells of the DCL do not form a continuous sheet but rather detach from one another and migrate individually spreading over the yolk. After completion of epiboly, there is no sign of an embryo, but the DCL contains dispersed cells that distribute over the yolk. At this stage, the *Austrolebias* embryo can follow one of two possible developmental routes: It can enter the first diapause and remain at this phase for an extended period (up to 8 months under our laboratory conditions; Miguel L. Concha and Soledad de la Piedra, unpublished); alternatively, cells of the DCL can start the reaggregation process and coalesce to build the embryo proper. In the following sections, we will focus on the process of reaggregation and early embryonic axis formation in *Austrolebias*. We will provide combined information obtained from *A. charrua* and *A. bellottii* embryos as they show similar patterns and speed of early embryonic development. When needed, we will specify the species where the information was obtained (i.e., for defining the duration of the stages of reaggregation and axis formation in Table 1).

Stages of Reaggregation in *Austrolebias* Embryos

Wourms (1972) described in detail the stages of reaggregation in *Austrofundulus myersi* using brightfield microscopy and also broadly compared the process of reaggregation among annual killifish species of several different groups, including *Austrolebias* (Wourms, 1972c). Although the process of reaggregation appeared strikingly similar in the different annual killifish species, no detailed spatial and temporal information was provided for the reaggregation process in *Austrolebias*. Thus, we first sought to define stages of reaggregation that could be later used as a reference for the interpretation of histological, cellular, and molecular analysis in this annual killifish species. We based our description on morphological features recognized by differential interference contrast (DIC) microscopy and combined this information with

TABLE 1. Stages of Reaggregation in *Austrolebias Charrua* and Their Main Features

Stage	Time (dpf)[a]	Characteristics: general, cell populations, cell size
100% ep	6	Deep blastomeres are dispersed over the egg and show diverse migratory-like morphology (filiform, bipolar, triangular).
RI	6.8	First signs of reaggregation: a small group of rounded cells (5–10) is surrounded by migratory cells (20–40) of diverse morphology and showing membrane protrusions such as filopodia and lamellipodia.
RII	7.25	Around 50 cells. Central cells (20–30 μm in diameter) organize as a monolayer and are surrounded by many migratory cells.
RIII-e	7.9	Around 100 cells, with morphology and size similar to that of RII. Some central cells adopt deeper positions in the reaggregate. Migratory cells at the periphery.
RIII-i	9.4	Around 200 cells, organized in central (∼10%) and peripheral (∼90%) populations. Central cells are small (∼15 μm diameter) and organize as a multilayer. Peripheral cells are rounded and large (25–35 μm diameter) and form a monolayer. Some large migratory cells are observed at the periphery. This is the longest stage of reaggregation (∼35 hrs).
RIII-l	10	Circular reaggregate ∼300 μm in diameter, with cells organized as in RIII-i. The central area of small cells covers ∼20% of the total area.
RIV	10.6	Circular reaggregate ∼450 μm in diameter, with cells organized as in RIII-l. The central area of small cells (∼10 μm diameter) covers 50%–70% of the total area; cell borders are not easily recognized. Peripheral large cells (∼20 μm diameter) form a ring-like structure.
RV	11.5	Elliptical reaggregate with long and short axes of ∼500 μm and 300 μm, respectively. Peripheral cells (∼10 μm diameter) form a horseshoe and concentrate at the prospective posterior end of the embryo.
Axis-e	11.7	First structures of the embryonic axis are observed. Two parallels folds 20 μm apart and connected posteriorly define the limits of the prospective notochord.
Axis-i	12.2	Embryonic axis grows bidirectionally along the anterior-posterior axis, reaching a length of ∼160 μm.
Axis-l	12.5	The entire axis is formed. Widening of the cephalic and caudal embryonic ends are visible.

[a]Time is in days post fertilization (dpf) at 25 degC. e, early; ep, epiboly; h, hours; i, intermediate; l, late; R, reaggregation. Measurement of cell diameter was estimated from populations of 5–15 cells.

3-dimensional (3D) volumetric reconstructions of confocal microscopy images to gain a better definition of the morphological events occurring along the *z*-axis of the reaggregate. For staging, we used the nomenclature proposed by Wourms (Wourms, 1972c), who divided the process of reaggregation into five stages, named reaggregate stages I to V (RI to RV). Given the long extension (> 65 hr) and major transformations observed in the reaggregation stage RIII, we further subdivided this phase into three substages named early (RIII-e), intermediate (RIII-i), and late (RIII-l). Below, and in Figures 1 and 2, we summarize the progressive changes exhibited by the cellular reaggregate during *Austrolebias* development. In Table 1, we describe the most relevant cellular and supracellular features that characterize each stage of reaggregation in *A. charrua*. We caution that the morphology of the different reaggregates (especially at early stages) is variable among embryos, and thus, the description corresponds to the most characteristic features observed in our samples.

The earliest manifestation of cell reaggregation is the formation of a small group of round-shape cells (5–10) surrounded by many migratory cells (stage RI, Fig. 1A and Table 1). This initial phase of reaggregation lasts for about 20 hr and is followed by a period of ∼10 hr in which cells accumulate within the reaggregate while forming a cell monolayer (stage RII, Fig. 1B and Table 1). In stage RIII, there is a progressive increase in the number of cells, particularly at the center of the reaggregate. In this central region, cells become progressively smaller in size likely due to events of cell division and start to organize as a multilayered structure. Peripheral cells, on the other hand, retain a large size and the organization of a monolayer (stage RIII, Fig. 1C–E, Fig. 2A, and Table 1). In stage RIV, the central area occupied by small cells progressively increases to fill up to 70% of the total area of the reaggregate within a period of ∼15 hr (stage RIV, Fig. 1F and Table 1). During this period, the organization of small cells at the center of the reaggregate becomes very compact, and the cell boundaries are not easily distinguishable. Also, the reaggregate starts to protrude deeply into the yolk as the multilayered organization of the central cell group increases (Fig. 2B). In the transition from stage RIV to stage RV, the shape of the reaggregate changes from circular to elliptical, and the peripheral cells begin to accumulate at the prospective posterior end of the embryo (Fig. 1G and Table 1). This change is the first morphological manifestation of anterior-posterior (AP) axial polarity within the reaggregate and is followed by the appearance of morphological features that define the embryonic axis, like the emergence of two parallel furrows that delimit the boundaries of the prospective notochord (Axis-e, Fig. 1H and Table 1). Later, the embryonic axis extends bidirectionally and an elongated neural axis with a widening in the anterior region is recognizable (Axis-l, Fig. 1I, Fig. 2C, and Table 1). At the latest stage analyzed in this study (seven somites), we could distinguish the process of segmentation of the paraxial mesoderm by the formation of the first somites on both sides of the prospective neural tube (Fig. 1J).

Histological Analysis of the Reaggregate

The initial morphological description revealed a gradual transformation of the reaggregate from a cell monolayer into a multilayered structure that protruded into the yolk and preceded the formation of

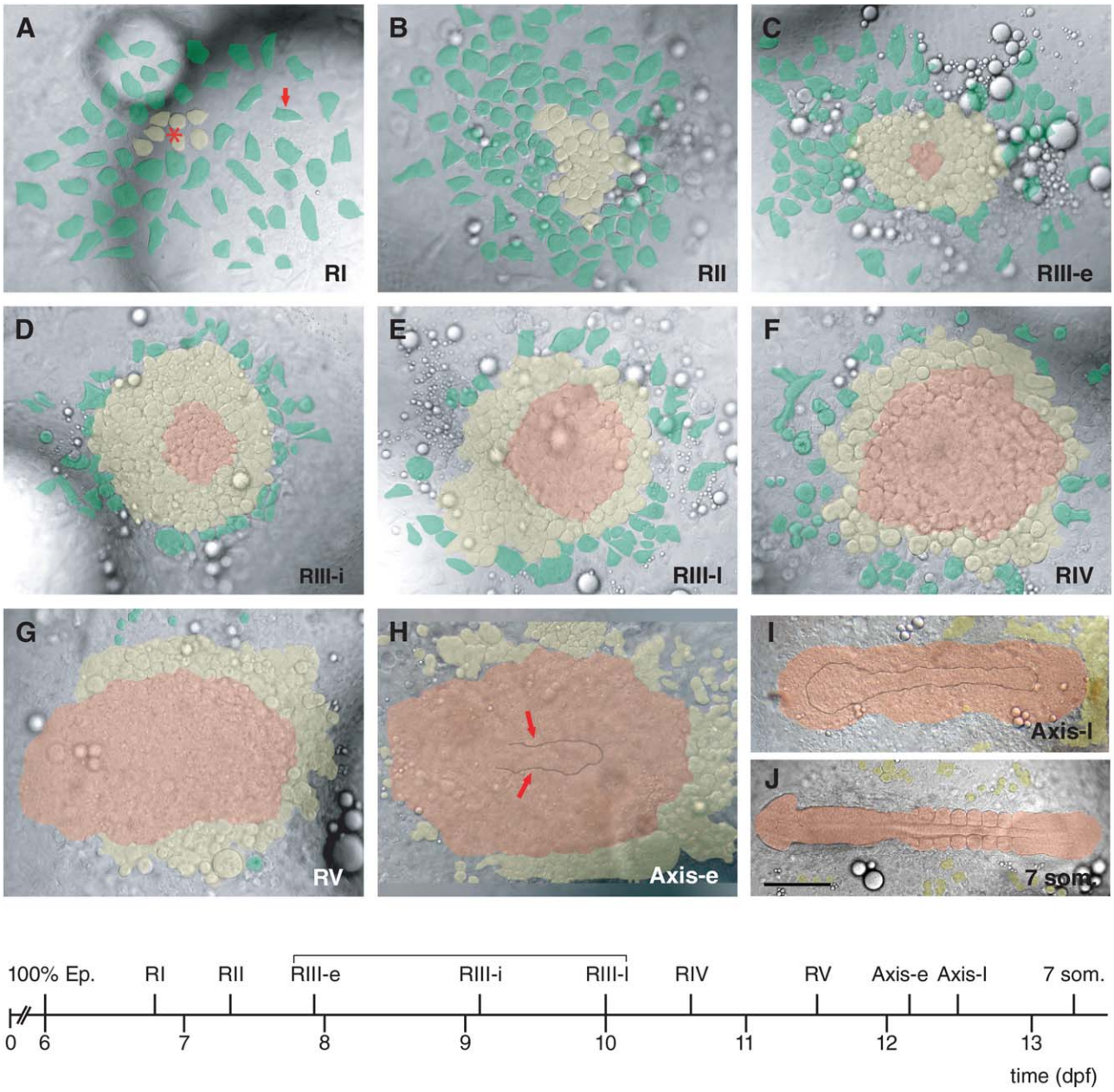

Fig. 1. Staging and timing of the cellular reaggregation process in *Austrolebias*. DIC microscopy images corresponding to surface views of embryos where cells have been pseudo-colored according to their position and shape within the forming cellular reaggregate. **A**: The first reaggregate (stage RI) consists of a small central group of rounded cells (yellow, asterisk) surrounded by stellate-shaped migratory cells (green, arrow). **B**: In the stage II of reaggregation (RII), the central and peripheral cells increase in number, but the reaggregate remains as a monolayer. **C–F**: The reaggregation stages III (early [RIII-e], intermediate [RIII-i], and late [RIII-l]) and IV (RIV) are characterized by a progressive increase in cell number, particularly in the center of the reaggregate. Central cells become progressively smaller in size, likely due to cell division, and organize as a multilayered structure (orange). Peripheral cells, on the other hand, retain their large size (green and peripheral yellow cells). **G**: The reaggregation stage V (RV) is characterized by a change in shape of the reaggregate from circular to elliptical. A monolayer of external cells (yellow) accumulates at the posterior end of the embryo and defines the first morphological manifestation of anterior-posterior (AP) polarity within the reaggregate. **H**: In the early embryonic axis stage (Axis-e), two parallel furrows delimit the notochord primordium (arrows). **I**: In the late embryonic axis stage (Axis-l), the axial mesoderm elongates along the AP axis. **J**: Seven-somite-stage embryo, with the cephalic region to the left. The timeline at the bottom shows the approximate times of the different stages of cellular reaggregation and embryonic axis formation. 100% Ep., 100% epiboly stage; dpf, days postfertilization. Scale bar = 100 μm.

the embryonic axis. To examine in more detail the changes in cell organization that accompany this transformation, we performed sequential semithin sections at a plane transversal to the surface of the embryo between stage RIII-i and three somites (Fig. 3). At stage RIII-i, the reaggregate appears as a disorganized group of cells with a lenticular distribution, occupying the space between the EVL and the YSL (Fig. 3E). A peripheral region containing a single cell layer can be distinguished from a central domain that contains several cell layers (4–5) (Fig. 3A,E). During stage RIV, the reaggregate continues to grow in thickness, in particular within its central region, but it is

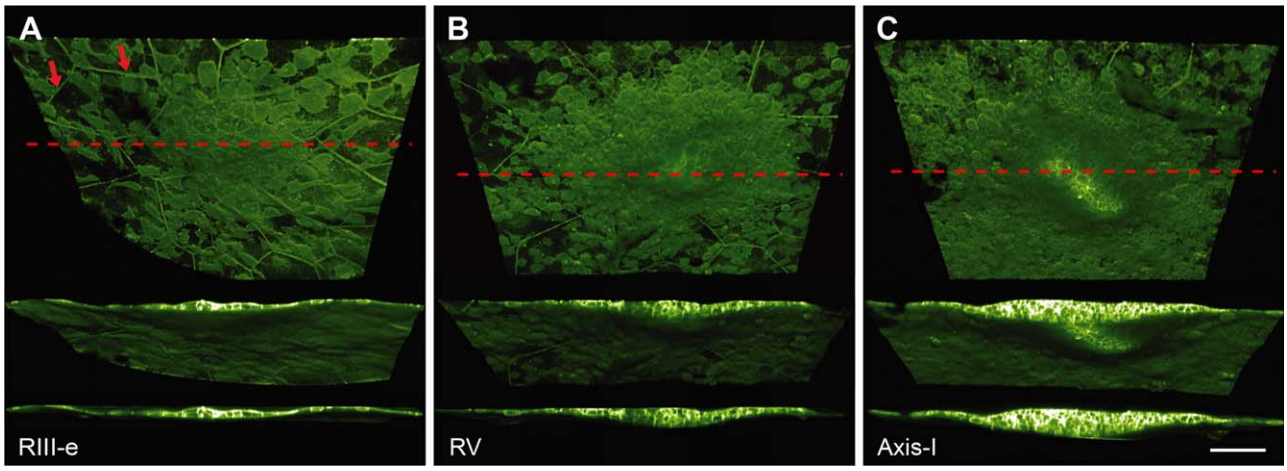

Fig. 2. Thickening of the cellular reaggregate and formation of the embryonic axis. Images correspond to confocal microscopy 3-dimensional (3D) volumetric reconstructions of *Austrolebias* embryos expressing membrane-tagged GFP at three different stages, defined in Figure 1. In the top panels, the 3D models are rotated to unveil the bottom part of the cellular reaggregate and embryonic axis. The reaggregate hides the superficial enveloping cell layer (EVL), and thus the cell membrane contours of this layer are visible only in lateral positions (arrows in A). The middle and bottom panels correspond to two different orientations of the same transverse optical sections taken along the red dashed lines depicted in the top panels. The EVL is toward the top, while the yolk cell is toward the bottom. The temporal progression shown in the three stages illustrates how the cellular reaggregate changes from a monolayer (RIII-e) to a multilayered (RV) structure, in particular within central positions, and then transforms into an elongated embryonic axis (Axis-I) that progressively protrudes deeply into the yolk cell (not labeled). Scale bar = 100 μm.

only at stage RV when the reaggregate appears more organized (Fig. 3B,F). At this stage, peripheral cells become compacted while cells at the center of the reaggregate form a circular structure ~70 μm in diameter (arrows in Fig. 3F), which likely corresponds to the presumptive notochord. At the late embryonic axis stage, the reaggregate shows more differentiated embryonic structures. For instance, a neural axis located above the notochord and flanked by the nonsegmented paraxial mesoderm is observed in a section through the middle of the embryo (Fig. 3C,G). Similarly, a midline-positioned circular structure that likely corresponds to the tail organizer is recognizable in a section across the caudal region of the embryo (Fig. 3C,H). Finally, at the three-somite stage, embryonic structures such as the neural keel, notochord, and somites appear further differentiated (Fig. 3D,I,J), and the presumptive tail organizer is still visible in the caudal region of the embryo (Fig. 3D,K).

Lineage Tracing of Reaggregate Cells

As the site of reaggregation, in particular, the central domain that changes from a monolayer into a multilayered structure coincides with the location where the embryonic axis later appears; we asked to which extent the cells of the reaggregate are fated to become axial embryonic tissues. To address this question, we performed lineage tracing based on the photoconversion of the Kaede protein (Ando et al., 2002). We injected one-cell stage embryos with Kaede mRNA and then UV-illuminated the entire or part of the reaggregate to photoconvert the fluorescence in cells from green to red, and then follow the fate of labeled cells later in development (Experimental Procedures and Table 2). Photoconversion of the reaggregate at stages RI (Fig. 4A–A''') and RII (Fig. 4B–B''') both led to similar results. Labeled cells were later excluded from the central core of embryonic cells and marginalized to the posterior periphery of the embryonic axis at early somite stages. These cells retained a larger size compared to the central cells and positioned on both sides of the embryonic axis in proximity to the somites but not forming part of them (Fig. 4A''',B'''). After photoconversion of the reaggregate at stage RIII-e, the majority of labeled cells were also excluded from the embryonic axis and became localized to the caudal end of the embryo at somite stages (Fig. 4C–C'''). However, a small proportion of labeled cells ended within structures of the embryonic axis such as the notochord (arrows in Fig. 4C'''). In successively later stages, the photoconversion of the reaggregate resulted in a progressive increase of the proportion of labeled cells becoming part of embryonic axial structures (Fig. 4D–D''' and 4E–E'''). For instance, when the central part of the reaggregate stage RIII-i was photoconverted, some labeled cells ended in neural tissues and somites (Fig. 4D–D'''). On the other hand, photoconversion of the central reaggregate at stage RV resulted in virtually all labeled cells forming part of the embryonic axis (Fig. 4E–E'''). In summary, the labeling experiments reveal a stereotyped temporal progression where cells of the early reaggregate (stages RI and RII) become extra-axial tissues (at least until early somite stages), while cells in successive stages of reaggregation (stages RIII to RV) progressively incorporate into structures of the embryonic axis. The apparent inability of cells of the early reaggregate to form axial embryonic tissue, however, should be taken with caution, as Kaede might have become diluted after successive rounds of cell division and thus remains undetectable under our observational conditions.

Expression of *Brachyury* and *Goosecoid* in the Reaggregate and Embryonic Axis

To start linking the process of reaggregation to embryonic axis formation, we examined the expression of molecular markers that are characteristic of the process of gastrulation in other vertebrate species. We carried out whole-mount in situ hybridization for two highly conserved genes of the early vertebrate gastrula: *brachyury* (*bra*), which is expressed in the presumptive mesoderm that forms the blastopore (Technau and Scholz, 2003), and *goosecoid* (*gsc*), which labels the embryonic organizer (Blum et al., 1992). Since

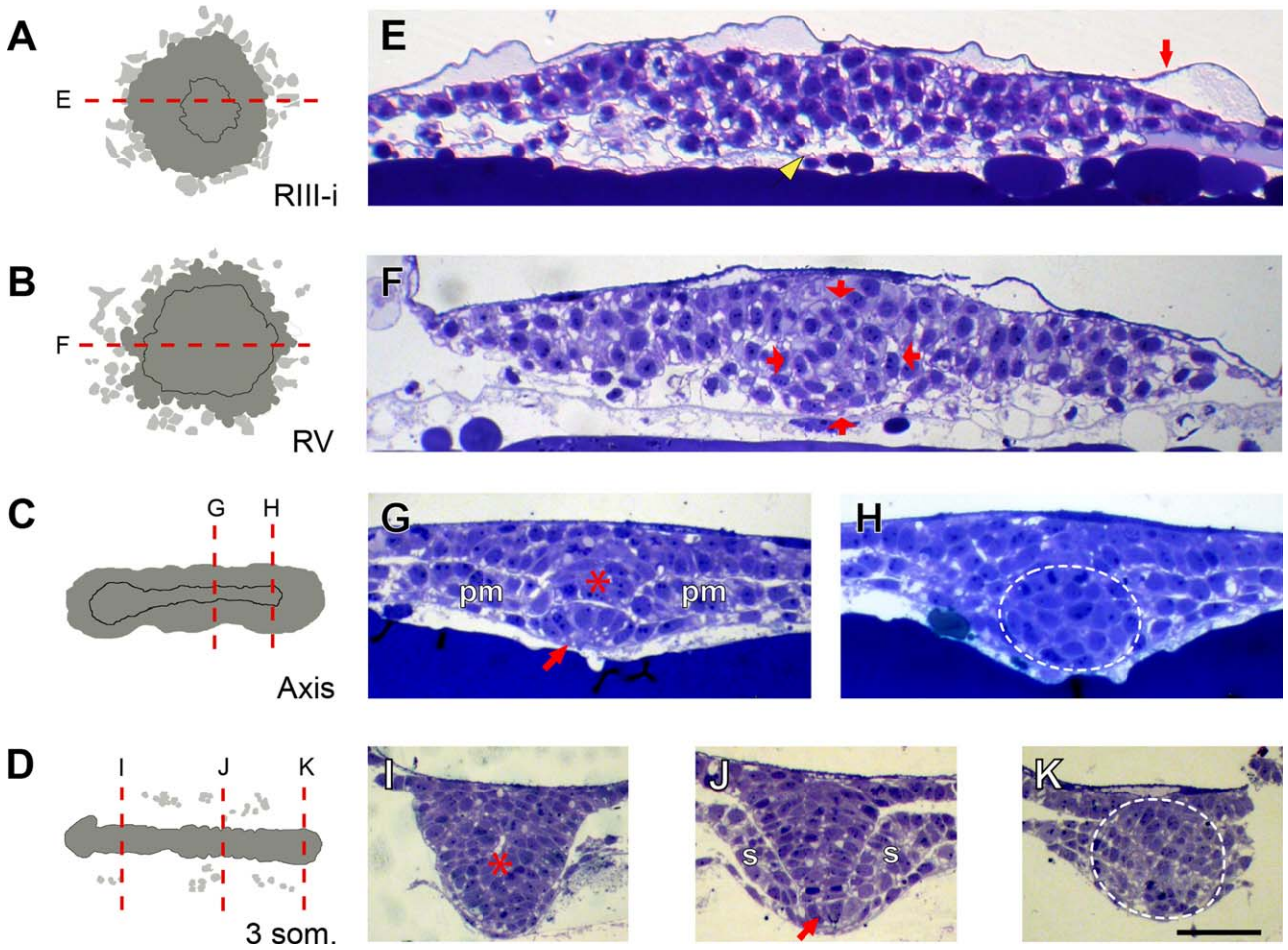

Fig. 3. Histological analysis of the cellular reaggregation process and embryonic axis formation. **A–D**: Schematic representations of different stages of reaggregation and embryonic axis formation, according to Figure 1, which illustrate the position of histological sections (dashed lines) shown in the right panels. Images E–K are representative transversal thick sections of Epon-embedded embryos stained with Toluidine Blue, with the superficial layer toward the top. **E**: The central part of the reaggregate at stage RIII-i consists of a multilayer of cells that apparently lack organization. The membranes of the enveloping cell layer (EVL, red arrow) and the yolk cell (yellow arrowhead) delimit the top and bottom surfaces of the cellular reaggregate, respectively. **F**: In the reaggregate stage RIV, cells organize into one to two layers at the periphery while they form an up-to-five-cell-layered circular structure at the center (arrows). **G,H**: In the embryonic axis stage, the notochord (arrow), paraxial mesoderm (pm), and forming neural keel (asterisk) are evident in a section through the middle of the embryo (G). A compact spherical structure (delimited by the dashed line) is distinguishable in a section through a caudal position. **I–K**: In the three-somite stage embryo, a neural keel (asterisk) is clearly observed in anterior (I) and middle (J) positions of the embryo. Notice that the somites (s) flank the neural keel, which lies above the notochord (arrow in J). In a section through a caudal position (K), a compact circular cellular structure (delimited by the dashed line), which likely corresponds to the tail bud, is observed. Scale bar = 50 μm.

gene sequences for *Austrolebias* were not available, we used a degenerate PCR primer strategy to clone short cDNA fragments belonging to both genes (see Experimental Procedures). These cDNA fragments showed high sequence homology to *bra* and *gsc* from other vertebrates (Supp. Fig. S1), and thus we use them to generate antisense probes to examine the expression of both genes in *Austrolebias* embryos.

The first expression of *bra* was detected at stage RIII-i in a circular domain, with *bra*-expressing cells distributed homogeneously (Fig. 5A). Later, at stage RIV, the expression of *bra* increased while maintaining a circular shape. When observed from a side view, the domain of *bra* expression appeared as an "inverted U," with central cells either lacking or showing low levels of *bra* expression, and marginal cells bulging toward deeper positions and forming a ring-like structure suggestive of a blastopore architecture (see histological section under Fig. 5B). At reaggregation stage RV, the general organization of *bra* expression was similar to stage RIV. However, its expression domain changed in shape from circular to elliptical (Fig. 5C), coinciding with the morphological changes observed within the reaggregate (Fig. 1F,G). Also, cells lacking (or showing low levels of) *bra* expression were no longer positioned at the center of the reaggregate but localized eccentrically toward the posterior end (dashed white line and asterisk in Fig. 5C). Finally, in the late embryonic axis stage, the expression of *bra* was missing from anterior regions and observed only in the posterior notochord and tail bud (Fig. 5D).

We next carried out double-whole-mount in situ hybridization to simultaneously examine the expression of *bra* and *gsc*. We observed that *gsc* expression started several hours after the onset of *bra* expression in the reaggregate; *gsc* was not detected in RIII-i embryos (Fig. 5E) but appeared only at stage RIII-l in a few cells that were positioned adjacent and in a more superficial position compared to *bra*-expressing cells (Fig. 5F). From stages of reaggregation RIV to

TABLE 2. Fate Map Analysis: Number and Characteristics of Experiments per Stage

Stage	Extent of photoconversion[a]	Fate of photoconverted cells[b]	N[c]
RI	50%	Extra-axial	6
RI	All	Extra-axial	6
RII	50%	Extra-axial	5
RII	All	Extra-axial	5
RIII-e	All	Extra-axial and embryonic	5
RIII-i	Central cells	Extra-axial and embryonic	4
RIII-i	All	Extra-axial and embryonic	4
RIII-l	Central cells	Mainly embryonic	5
RIV	Central cells	Mainly embryonic	3
RV	Central cells	Embryonic	3

[a]Photoconversion was achieved by illuminating with UV light circular regions that comprised the entire ("All"), half ("50%"), or only the central cells of the aggregate.
[b]Labeled cells were evaluated as to their eventual fate at the five-somite stage or later. "Extra-axial" refers to cells located outside of somite boundaries. "Embryonic" refers to cells within the axis (notochord, somites, or presumptive neural tissues).
[c]Total number of embryos analyzed

RV, the *gsc* and *bra* expression domains became progressively segregated along the AP axis, the former moving toward anterior while the latter toward posterior (Fig. 5G–K). Early in this process, at stage RIV-e, the domains of *gsc* and *bra* expression appeared to overlap in a small central region along the AP axis (arrows in Fig. 5G). Next, at stage RIV-i, *gsc*-expressing cells located deeper than *bra*-expressing cells at the region of contact between the two expression domains (arrows in Fig. 5H). Finally, the expression domains of *gsc* and *bra* gradually separated and became localized to the anterior and posterior ends of the embryonic axis, respectively (Fig. 5I–L). *gsc* expression was observed in the presumptive prechordal plate while *bra* was detected in posterior mesodermal tissue (e.g., posterior notochord and tail bud) (Fig. 5K). In the latest stage analyzed, the three somites, *bra* labeled the tail bud while *gsc* was restricted to the very anterior end of the embryo (Fig. 5L).

Cellular Movements During Early Stages of Reaggregation

To explore the cellular movements that characterize the morphological and molecular transformation of the reaggregate, we took advantage of the transparency of *Austrolebias* embryos and performed in vivo microscopic imaging. For this, we injected one-cell stage embryos with mRNA coding for both membrane-tagged GFP and nuclear-localized RFP and then performed 4-dimensional (4D) confocal microscopy in living embryos at different stages of reaggregation. As the process of reaggregation lasts for over five days in *Austrolebias*, we were unable to carry out a continuous observation across all stages. Furthermore, the possibility of imaging the onset of reaggregation was unrealistic, as no landmark pointed to the position where the reaggregate will form. For these reasons, we focused on capturing the global changes of cell behavior in two specific temporal windows. First was the transition from stage RII to RIII-i (Fig. 6A and Supp. Movie 1, spanning 31 hr). Second was the transition from RIII-e to RIII-i (Fig. 6B,C and Supp. Movie 2, spanning 15 hr). Also, we performed high-resolution imaging of cell behavior for short temporal windows within the reaggregate at stage RIII-i (Fig. 6D–L and Supp. Movies 3, 4 and 5, spanning 5.5 hr).

At reaggregation stage RII, the central and peripheral cells of the reaggregate showed distinct behaviors. Central cells were closely packed, rounded, or polyhedral and showed little migratory activity (Fig. 6A, box 1, and Supp. Movie 1). In contrast, peripheral cells migrated actively between the surface of the yolk and EVL (Fig. 6A, box 2, and Supp. Movie 1). These cells were large (cell diameter: $60 \pm 7\,\mu m$; $n = 20$) and displayed features characteristic of mesenchymal-like migratory cells, adopting different shapes (bipolar, filiform, triangular) and showing prominent membrane protrusions in the form of lamellipodia and filopodia. The movement of these cells was not directional but instead displayed circular trajectories and frequent events of cell-to-cell collision, characteristic of a process of contact inhibition of locomotion (Fig. 6A, box 2, Supp. Movie 1). A second less frequent group of migratory cells at this stage were rounded, produced multiple membrane blebs and moved nondirectionally (Fig. 6A, box 3, Supp. Movie 1).

Noticeable changes in cell behavior were observed in the transition from reaggregation stage RII to stage RIII. The central region appeared less homogeneous and contained a mixture of large and small cells moving and translocating actively between each other (Fig. 6B, Supp. Movie 2). Also, the shape of the reaggregate changed from irregular and loose to circular and compacted as the stage RIII progressed (Fig. 6C, Supp. Movie 2). As suggested by the previous lineage-tracing experiments (Fig. 4C–C''', 4D–D'''), the two cell types observed in the RIII likely correspond to the cells that later become nonaxial (large cells) and axial (small cells) structures. However, from our movie, which lasted only 15 h (the entire RIII stage is about 65 hr), we were unable to follow the fate of these cells until the embryonic axis stage, nor we could distinguish if these cells showed a defined pattern of collective movement. In spite of these limitations, we noticed a centripetal movement where small cells, which initially appeared more dispersed, progressively accumulated at the center of the reaggregate and became surrounded by large cells (Fig. 6C, Supp. Movie 2).

To further investigate the mechanism underlying the formation of multiple cell layers within the reaggregate, we performed high-resolution 4D confocal microscopy and tracked a subset of

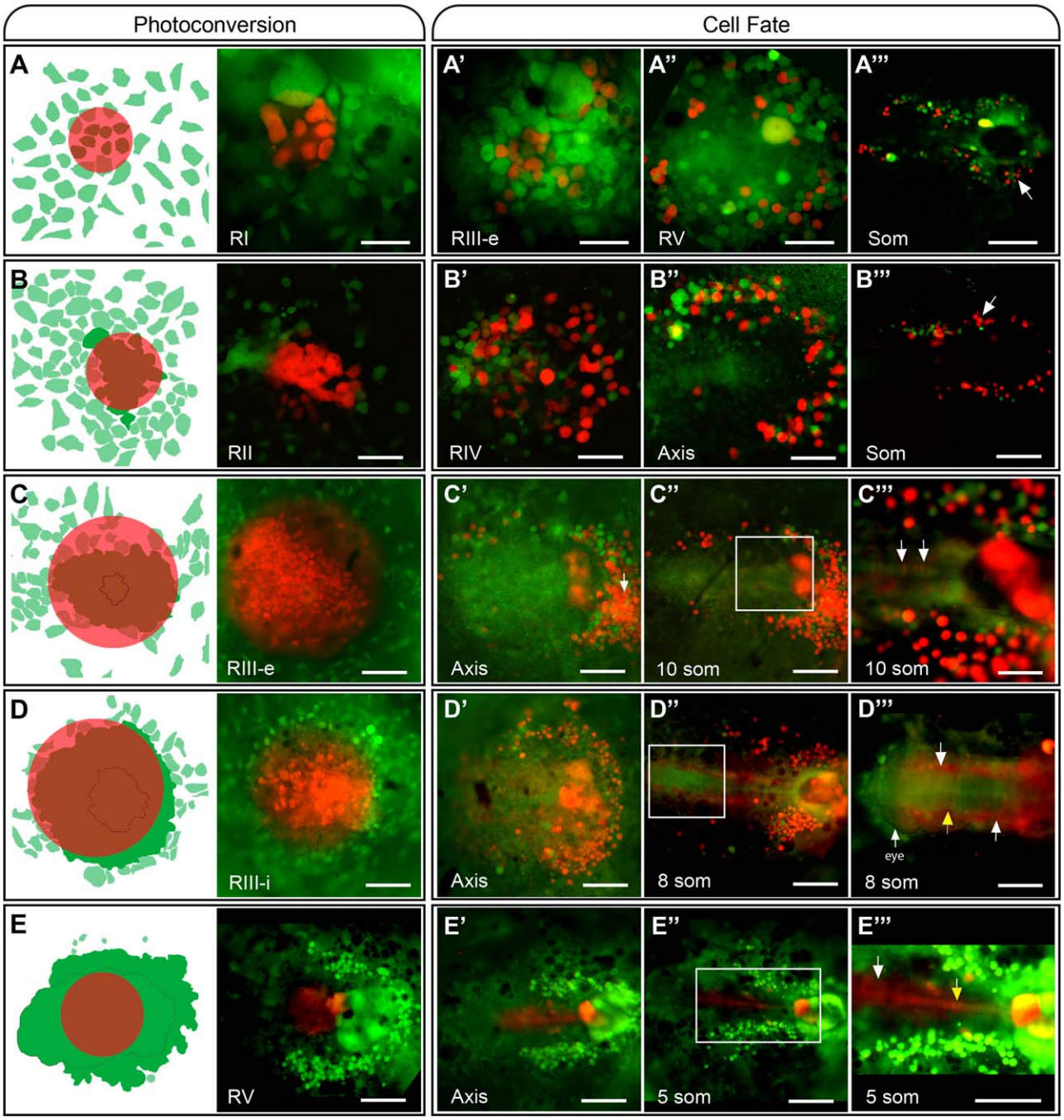

Fig. 4. Analysis of cell fate in the forming cellular reaggregate. **A–E**: Schematic representations (left, according to Fig. 1) and epifluorescence microscopy images (right) of embryos expressing Kaede at different stages of reaggregation, which illustrate the circular area of UV-mediated photoconversion. After photoconversion, the fluorescence of Kaede shifted from green to red. **A'–E', A"–E", A'"–E'"**: Fluorescence microscopy images showing the distribution of photoconverted cells (red) in the same embryos as in A–E but at later stages of reaggregation and embryonic axis formation (indicated in the left bottom corner of each panel). **C'"–E'"** correspond to high-magnification views of the square regions depicted in **C"–E"**, respectively. **A–A"**: Photoconverted cells at the center of the reaggregate stage RI move to the periphery, toward lateral and posterior positions (arrow), and do not appear to form part of any structure of the embryonic axis, at least until early somite stages. **B–B'"**: Photoconverted cells at the center of the reaggregate stage RII show a similar behavior as in A–A'", although more cells are labeled in the same area due to their smaller size. Peripheral cells are large and apparently undergo little cell division. Cells that form part of the embryonic axis, on the other hand, become progressively smaller in size due to cell division. Because in this condition Kaede could dilute and become undetectable by conventional epifluorescence microscopy, we can not rule out that some undetected photoconverted cells become part of the embryonic axis. **C–C'"**: Photoconversion of the majority of cells within the reaggregate stage RIII-e results in cells located in both the posterior periphery of the embryo (large cells, arrow in C') and the embryonic axis (small cells, arrows in C'") at later developmental stages. **D–D'"**: Photoconversion of the majority of cells forming the reaggregate stage RIII-i leads to similar results as in C–C'", although the proportion of cells within structures of the embryonic axis is much higher. In the eight-somite-stage embryo shown in D" and D'", photoconverted cells appear on both sides of the neural axis (white arrows), and some even within the neural tube (yellow arrow); the forming eye is shown. **E–E'"**: Photoconverted cells at the center of the reaggregate stage RV become mostly incorporated within the embryonic axis at later stages (arrows in E'"). White and yellow arrows point to labeled cells in the neural axis and notochord, respectively. Images in all panels are surface views of the embryo with posterior to the right, except for the stages in which the anterior-posterior axis can not be distinguished by morphology (A,B,C,A'). Scale bars for all panels except C'" and D'" = 150 μm. Scale bars for C'" and D'" = 50 μm.

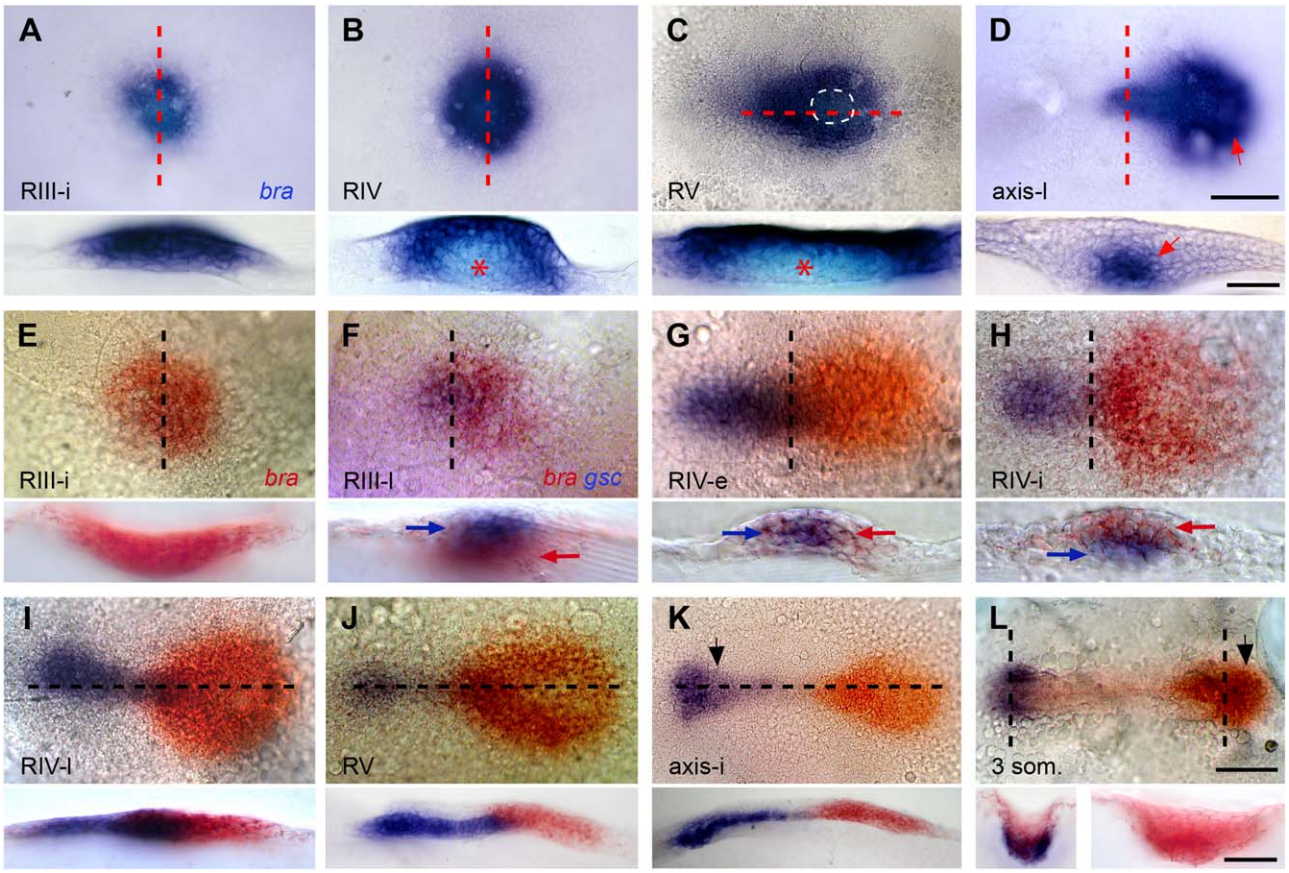

Fig. 5. Expression pattern of *brachyury (bra)* and *goosecoid (gsc)* during embryogenesis of *Austrolebias*. Whole-mount in situ hybridization was carried out in embryos fixed at the indicated stages using a single probe (purple stain for *bra* in panels A–D) or two probes (red stain for *bra* and purple stain for *gsc* in panels E–L). For all panels, upper rows are surface views with anterior to the left, except in A, B, and E, in which the anterior-posterior (AP) axis can not be recognized. Lower rows are transverse histological sections of the embryos shown in the upper images (plane indicated by dashed lines). **A**: In the reaggregate stage RIII-i, the expression of *bra* shows a circular pattern. Cells expressing *bra* are distributed homogeneously in all depths of the reaggregate as seen in the section. **B**: In the reaggregate stage RIV, *bra* expression still has a circular shape but is not homogeneous. From a side view, the central-most cells within the reaggregate either lack or show low levels of *bra* expression (asterisk). **C**: In the reaggregation stage RV, *bra* is expressed in an elliptical pattern with cells in the central and posterior zone of the reaggregate either lacking or showing low levels of *bra* expression (white dashed line and asterisk in the section below). In the histological sections associated with B and C, it is possible to observe that cells located at the margin of the *bra* expression domain adopt deeper positions compared to central cells, forming an inverted U, suggestive of a blastopore-like architecture. **D**: In the late embryonic axis stage (Axis-l), *bra* is expressed in the posterior notochord and tail bud (arrow). The transversal section shows the expression in the notochord (arrow in bottom panel). **E**: In the reaggregation stage RIII-i, *bra* expression shows a circular pattern (as in A), but *gsc* is still not detected. **F**: In the reaggregation stage RIII-l, *gsc* starts to be expressed in a few cells that are offset about the *bra* expression pattern, indicating the presumptive organizer region and anterior pole of the embryo. In the section, it is possible to observe that *gsc*-expressing cells (blue arrow) show a more superficial position within the reaggregate compared to *bra*-expressing cells (red arrow). **G**: In the reaggregation stage RIV-e, the expression domains of *gsc* and *bra* become segregated toward anterior and posterior positions, respectively. The section shows that in a transition zone along the AP axis, the expression of *gsc* (blue arrow) and *bra* (red arrow) partially overlaps. **H**: In the aggregation stage RIV-i, *gsc* and *bra* expression domains continue to separate, but in the transition zone, the cells expressing *gsc* (blue arrow) adopt a more ventral position than those showing *bra* expression (red arrow). **I–L**: At later stages of reaggregation (RIV-i and RV) and during embryonic axis formation (Axis-i and 3 somites), *gsc* and *bra* expression domains separate until they are no longer connected. At the intermediate embryonic axis stage (K), *gsc* labels the prechordal plate (pcp). In the latest stage analyzed (L, three somites), the cells expressing *bra* concentrate in the tail bud (arrow in L) and *gsc*-expressing cells label the presumptive forebrain. While some traces of red staining (*bra*) are observed, these are most likely nonspecific labeling, as the more sensitive purple stain used in panel D failed to reveal any anterior expression of *bra* at this stage. Scale bars for A–D, top panels = 100 μm. Scale bars for E–L, top panels = 50 μm. Scale bars for A–L, bottom panels = 30 μm.

individual cells for a period of 5.5 hr starting at stage RIII-i. Out of one movie, three different close-up frames were selected to highlight three characteristic cell behaviors (Fig. 6D–L, Supp. Movies 3, 4, and 5). Cells located in the center of the reaggregate displayed polyhedral cell morphology with no evident membrane protrusions. In the plane parallel to the embryo surface, we observed individual cells diminishing their surface area until they were no longer visible, the space left behind being replaced by neighboring cells. This behavior was suggestive of a process of internalization or ingression (Fig. 6D–F, Supp. Movie 3). On the contrary, some cells emerged in the surface plane from deeper positions as their area progressively increased and neighboring cells were displaced (Fig. 6G–I, Supp. Movie 4). During the entire length of this time-lapse sequence (5.5 hr), we observed 35 events of cell internalization or appearance. Additionally, we observed cells moving between the immediate neighbors along the surface plane, a behavior reminiscent of a process of planar cell intercalation (Fig. 6J–L, Supp. Movie 5).

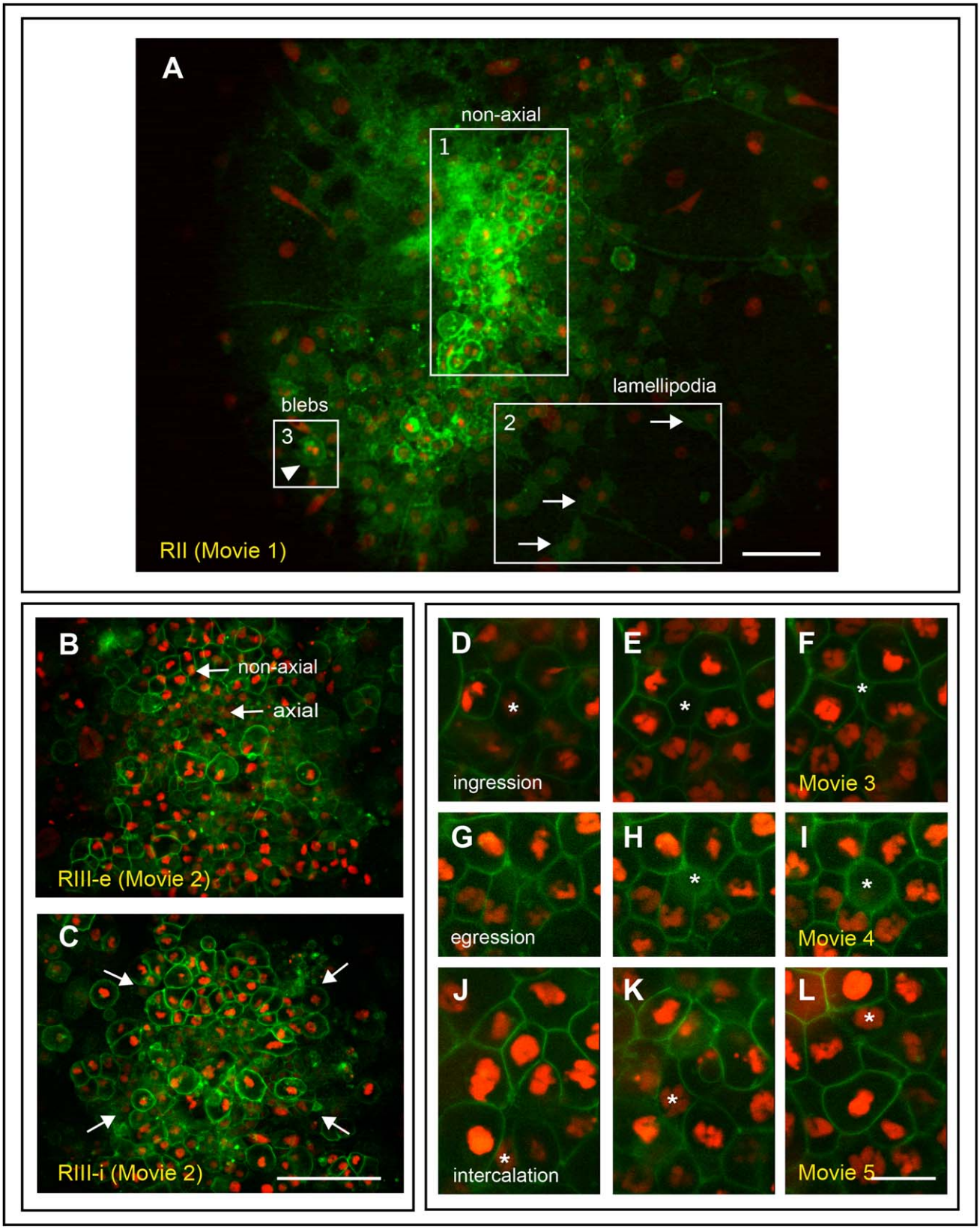

Fig. 6. Cell behavior during the early stages of reaggregation. Panels correspond to surface views of confocal microscopy images taken from *Austrolebias* embryos expressing membrane-tagged GFP (green) and nuclear-localized RFP (red). Images were captured at the indicated stages and time-lapse sequences were compiled (see Supp. Movies). **A**: In a picture of the reaggregation stage RII, the positions of three distinct cell morphologies are indicated by the boxed areas 1 to 3. **Box 1**: First cells forming the reaggregate, which later move toward lateral and posterior positions and become excluded from the embryonic axis. **Box 2**: Migratory cells in the periphery of the reaggregate extending filopodia and lamellipodia (arrows). **Box 3**: Cells actively forming blebs (arrowhead). **B,C**: Centripetal movement of cells from RIII-e (B, t = 1) to RIII-i (C, t = 31). In the reaggregation stage RIII-e, large polyhedral cells (prospective nonaxial cells) surround the periphery of the reaggregate while small cells (prospective embryonic axis) distribute among the nonaxial cells. Later, in the reaggregation stage RIII-i, a centripetal movement of axial cells can be detected, while nonaxial cells remain at the periphery. Also, compaction of the reaggregate is evident (aggregate delimited by arrows). **D–F**: Time-lapse sequence showing a cell leaving the surface toward deeper positions (asterisks). **G–I**: Time-lapse sequence showing a cell emerging toward the surface from deeper positions (asterisks). **J–L**: Time-lapse sequence showing a cell moving between two neighboring cells along the surface plane (asterisks). Scale bars for A = 100 μm. Scale bars for B,C = 50 μm. Scale bars for D–L = 20 μm.

Discussion

This work describes, for the first time, the process of early development leading to embryonic axis formation in an annual killifish, incorporating gene expression markers, cell-labeling techniques, histological sections, light and fluorescence microscopy, and 4D in vivo confocal imaging. In the specific case of *Austrolebias* embryos, applying these methods was challenging given that it is not an established laboratory model, that embryos are difficult to obtain and few in number, that the thick chorion is an obstacle for live imaging and microinjection, and that development is exceedingly slow compared to that of other established fish models such as Zebrafish or Medaka. Nonetheless, we present here a first description of the process of gastrulation in this species, which is unlike that of the other teleosts studied thus far.

Cells of the Early Reaggregate Appear Unique Among Teleosts

From our morphological, labeling, and molecular data, we could recognize that the reaggregate of *Austrolebias* is a heterogeneous cell group that dynamically changes in behavior and fate as it progresses from early to late stages of reaggregation. At early stages (RI and RII), the reaggregate is formed primarily by mesenchymal-like migratory cells that move with random trajectories and surround a small group of nonmigratory compacted central cells. Neither peripheral nor central cells express molecular markers indicative of gastrulation or embryonic axis formation (*bra* or *gsc*), nor do they appear to be fated to form part of any recognizable axial embryonic structure (somites, neural tube, or otherwise). Instead, most (if not all) of these cells are excluded from the central core of embryonic cells as development proceeds and become localized to the posterior margin of the embryo during axis and early somite stages. This finding is unexpected and raises the intriguing possibility that the early reaggregate is a type of extraembryonic tissue. The gradual exclusion from the central core of the reaggregate, where prospective embryonic cells congregate, also suggests that cells of the early reaggregate might play directive roles in the process of reaggregation, possibly acting as a recruiting center for the continuing arrival of more cells. These cell behaviors are reminiscent of those described for extraembryonic tissues of amniote embryos, in which the hypoblast of chick and the anterior visceral endoderm (AVE) of mouse exhibit morphogenetic movements along the AP axis and play fundamental roles in controlling the time and site of gastrulation (Stern and Downs, 2012). In teleosts, the YSL is an extraembryonic tissue with similar functions to the chick hypoblast and mouse AVE, as shown by Zebrafish work (Ho et al., 1999; Solnica-Krezel and Driever, 2001). However, in annual killifish, the role of the YSL is yet unexplored. Whether the early reaggregate described here is indeed extraembryonic and plays directive functions in the process of reaggregation and gastrulation, either independently or downstream the YSL, awaits further extended fate map, molecular, and functional analysis through physical and genetic ablation. It is possible, though, that when testing these hypotheses, we resolve that the nonaxial nature of the early reaggregate is simply a manifestation of a specialized tissue fate (e.g., germ cells) that colonizes the embryo only at late stages of development.

Gastrulation Occurs in the Central Region of the Reaggregate

In contrast to peripheral cells, the central region of the reaggregate in annual killifish undergoes a set of morphological and molecular changes from stage RIII onward that appears directly related to the formation of the germ layers and embryonic axis: 1) It increases the total area and number of cells, likely due to a combination of cell division (revealed by the progressive reduction in cell size) and the inward movement of peripheral regions (shown by the observation of centripetal movements within the reaggregate). 2) It increases the organizational complexity as it changes from a cell monolayer into a thick multilayer that starts to protrude into the yolk. The underlying mechanism of this transformation is not completely understood, but our 4D imaging studies revealed that, in addition to cell division, there is a contribution of inward movements and individual events of cell ingression, emergence, and intercalation. 3) Cells start to acquire embryonic axis fate, a feature that progresses as cell number increases in the central region of the reaggregate. Finally, 4) the reaggregate begins to express molecular markers such as *bra* and *gsc*, which typically label the presumptive blastopore and organizer regions, respectively. Altogether, these observations indicate that the central area of the reaggregate in *Austrolebias*, in particular after stage RIII, becomes progressively engaged in molecular and morphogenetic transformations, suggestive of a process of gastrulation and embryonic axis formation.

Is the Reaggregate Equivalent to the Embryonic Shield of Non-annual Teleosts?

The cycle of dispersion and reaggregation of annual killifishes shares similarities with cellular processes described in embryos of non-annual teleost species (Wourms, 1972c). In particular, a phase of partial "disengagement" of the deep blastomeres that is followed by subsequent convergence and accumulation is observed in the formation of the "nubbin" (prospective prechordal plate) in *Salmo Salvelinus* (Ballard and Dodes, 1968) and the embryonic shield in *Oryzias latipes* (Yokoya, 1966) and *Fundulus heteroclitus* (Wourms, 1972c). Wourms (1972c) proposed that embryogenesis, as it occurs in the reaggregate of annual killifishes, is equivalent to the events taking place in the embryonic shield of non-annual teleosts. The results presented here indicate that a parallel between the two processes (reaggregation and shield formation) is only partial. Regarding overall behavior, the circular shape, centripetal movements, increase in cell layers leading to bulking into the yolk, the events of single-cell ingression, and the expression of *bra* and *gsc* are all present in the formation of the reaggregate and embryonic shield (Montero et al., 2005). Note, however, that cell density is much lower in the early reaggregate than in the initial shield, and that the subsequent increase in size is driven by cell divisions and movements in the former (this study and Wourms, 1972c), with cell movements playing a key role in the latter (Warga and Kane, 2003; Montero et al., 2005). Also, the initial area of *gsc* expression is considerably smaller in the reaggregate than in the shield (compare Fig. 5F with Fig. 1 of Montero et al., 2005). The superficial position of *gsc* compared to *bra* within the reaggregate (Fig. 5F) might be indicative of an early stage of gastrulation, as the expression of this gene later adopts a deeper position compared to *bra* (Fig. 5G,H), possibly due to cell internalization within the organizer

region, as observed in the shield of Zebrafish (Montero et al., 2005). A final and important difference is that the expression domain of *bra* in the reaggregate is not connected at lateral positions to a ring of *bra*-expressing cells embracing the whole circumference of the egg (at least at levels detectable by whole-mount in situ hybridization), as seen in the Zebrafish shield (Schulte-Merker et al., 1994). Together, the comparison of the reaggregate in *Austrolebias* with the embryonic shield in Zebrafish allows us to make two important conclusions: First, the reaggregate likely contains (but it is not solely formed by) an organizer region that is positioned at one edge of a compressed blastopore-like structure labeled by *bra* expression. Second, the cells engaged in gastrulation movements in annual killifishes appear to primarily arise from the reaggregate in contrast to Zebrafish, where cells outside the embryonic shield contribute significantly to the gastrulation movements (Kane and Adams, 2002). Whether and to what extent lateral cells migrate into the reaggregate of annual killifishes to engage in gastrulation movements is yet unknown and will become clear from in vivo imaging studies comprising the whole embryo.

A New Mode of Gastrulation in Annual Killifishes

Comparative studies in vertebrates have revealed that the process of germ layer formation during gastrulation takes place in one of two structural variants. It organizes along a longitudinal thickening with a central furrow, as in most amniotes, or through a circular cleft (blastopore) between the animal and the vegetal hemisphere, as seen in amphibians and fishes (Keller et al., 2003; Tam and Loebel, 2007; Solnica-Krezel and Sepich, 2012). Our analysis of *bra* expression in *Austrolebias* reveals that the annual killifish pattern of gastrulation is reminiscent of a blastopore architecture but with significant morphogenetic variations. The first expression domain of *bra* is not a ring but circular in shape. As development proceeds, the outer margin of the *bra* expression domain appears to bulge inward, adopting a ring-like appearance. However, no sign of collective internalization movements at the peripheral margin is observed, as expected for a blastopore (Keller et al., 2003). In contrast, cells exhibit scattered events of single-cell internalization combined with events of emergence and intercalation along the surface plane. Although these observations do not exclude the possibility that a small blastopore forms at the periphery of the reaggregate, they do suggest that the pattern of morphogenetic movements critically differs from the coordinated cellular movements seen in the blastopore of most other animals, including modern teleosts such as Zebrafish (Kane and Adams, 2002). As the mechanics of cell internalization is highly variable among vertebrates, it is possible that gastrulation in annual killifishes is driven by events of single-cell ingression/delamination without large-scale movements, as observed during mouse gastrulation (Williams et al., 2012). Also, oriented cell divisions might play a role, as seen in the formation of the primitive streak in birds (Wei and Mikawa, 2000). We must caution, however, that a technical limitation of our in vivo image analysis is the inability to continuously image the whole process of reaggregation due to the slow development of *Austrolebias* embryos. Thus, we can not rule out that a coordinated blastopore-like pattern of cell internalization might emerge within the reaggregate after tracking the trajectory of all cells in longer-term high-resolution 4D observational studies like those using adaptive light-sheet microscopy (Royer et al., 2016).

Despite showing different morphologies, the polarity and territories of the early gastrula share significant homologies among vertebrate species, including model and nonmodel organisms. For instance, it has been proposed that the dorso-ventral polarity of amphibians and teleosts are evolutionarily linked to the embryonic-extraembryonic organization of the dogfish (a chondrostean) and amniotes (Coolen et al., 2007). Also, within amniotes, differences in the mode of gastrulation from blastopore-like in reptiles to the formation of a primitive streak in birds and mammals seem largely morphogenetic, while the cellular sources and dorsal-ventral patterning of the endoderm and mesoderm are very similar (Bertocchini et al., 2013). Here we show that from a structural viewpoint, gastrulation in annual killifishes shares the ancestral blastopore-like architecture, but with significant variations. An important source of variation is morphogenetic, although future studies will determine if additional modifications involve the role of extraembryonic tissues and the origin and patterning of the endoderm and mesoderm.

Evolutionary Forces Driving the Annual Killifish Mode of Gastrulation

The temporal separation of gastrulation from epiboly, the extremely low cell density of the DCL, and the spatial restriction of gastrulation to a small cellular reaggregate on the surface of a large yolk appear as key determinants for transforming the mode of gastrulation in annual killifishes, and make this process so different from non-annual teleost species. The yolk cell of *Austrolebias* measures about 1mm in diameter, compared to the 0.7mm in diameter of the Zebrafish yolk cell. However, at the start of epiboly, Zebrafish embryos have at least 10 times more cells than *Austrolebias* (Kimmel et al., 1995; Arezo et al., 2005). Thus, in Zebrafish, epiboly of the DCL proceeds as a vegetal displacement of a sheet of cells, and the overlap of this movement with gastrulation requires involution/ingression as the sheet moves over the yolk (Warga and Kimmel, 1990). In contrast, the *Austrolebias* layer of deep cells must spread out over a similar surface but with 10 times fewer cells, causing the cells to break contact with one another soon after epiboly begins (Wourms, 1972c; Carter and Wourms, 1991). Since gastrulation is delayed with respect to this movement, there is no involution nor formation of germ layers during epiboly. The only course of action left is for the dispersed cells to reaggregate in a small domain of a large egg and to gastrulate separately from the epiboly stage. How did molecular, cellular, and developmental mechanisms evolve to initiate and drive the progression of morphogenesis toward embryo formation in annual killifishes? The extraembryonic YSL appears as a good candidate to launch the reaggregation process, as it provides signals that position the organizer in Zebrafish in a way reminiscent to the Nieuwkoop center of amphibian embryos (Ho et al., 1999; Solnica-Krezel and Driever, 2001). Supporting the idea of an external initiation source, the position of the reaggregate is not random but forms primarily in the vegetal hemisphere of the egg (Wourms, 1972c). Once reaggregation has started, the next critical step is to reach a minimal/optimal cell mass for further progression into gastrulation and embryonic axis formation. This goal seems to be achieved in annual killifishes via cell division and the immigration of cells from peripheral regions. Recent developmental studies and embryonic stem cell in vitro work have shown that a minimal/optimal multicellular organization and geometrical confinement are required to recapitulate early embryonic development in a vertebrate (Bedzhov and

Zernicka-Goetz, 2014; van den Brink et al., 2014; Warmflash et al., 2014). In particular, a recent study revealed that under defined culture conditions and cell numbers, aggregates of mouse embryonic stem cells (mESCs) undergo gene expression and morphogenetic processes that resemble the in vivo behavior of cells during mouse gastrulation, for instance, the polarized expression of *bra*, the delamination of cells from the aggregate, and the establishment of axial structures (van den Brink et al., 2014). This study also suggested that self-organizing properties could promote the symmetry-breaking events observed in the aggregates of mESCs, and that external signals from extraembryonic tissues could serve to direct this process and make it reproducible (van den Brink et al., 2014). Although it is probably premature to speculate about the mechanisms driving gastrulation in the reaggregate of annual killifishes, it is possible that self-organizing properties play a fundamental role and that extraembryonic tissues such as the YSL (and possibly the early reaggregate described here) provide signals to direct this process. Importantly, annual killifish embryos allow these hypotheses to be tested experimentally in the future.

Conclusions and Perspectives

Given its phylogenetic position, *Austrolebias*, as well as other annual killifish, must undergo developmental processes that are related to those of other teleosts. The dissimilar appearance of the early embryo between annual killifish and other non-annual teleost fishes appears to obey to three fundamental constraints: 1) the temporal uncoupling between the processes of epiboly and gastrulation; 2) the low number of deep cells at the beginning of gastrulation; and 3) the spatial restriction of the gastrulation process to a small domain on the surface of a large yolk. The result is the acquisition of a unique embryonic architecture when gastrulation is set to occur: the reaggregate. A remarkable conclusion from this type of development is that a process so ancient and fundamental to animal life as gastrulation has room for more variation in mechanism than could be predicted from the examination of a few species. Moreover, it is likely that the unique environmental constraints and selective pressures that occurred during the evolution of annual killifishes are the forces behind such specialization, molding developmental pathways while leaving adult morphology substantially unaltered.

We focused on the events that transpire in the reaggregate, at stages that precede the formation of an axis, because at the axis stage, structures are recognizable and homologous to those of other fish. Our work provides a preliminary glimpse into a very complex phenomenon that has been resistant to analysis via traditional means, such as genetics and transgenesis for examining gene function and cell lineage. We show that *Austrolebias* embryos gastrulate with extremely divergent morphological features. The reaggregate is the cellular substrate for gastrulation and exhibits two main developmental transformations. First, it appears to recruit nonaxial tissue of possible extraembryonic nature, which might play a role in the further recruitment of embryonic cells. Then, the reaggregate engages in molecular and morphogenetic transformations proper of gastrulation and embryonic axis formation. The analysis of molecular markers such as *bra* and *gsc* suggests that the reaggregate contains but is not solely formed by an organizer region, which locates toward one end of a compressed blastopore-like structure. No collective cell internalization proper of blastopore architecture is observed, though, and it appears that gastrulation in annual killifishes primarily involves the reorganization of individual cells. Thus, gastrulation in annual killifishes appears to share the ancestral blastopore-like architecture present in most vertebrate species, but with significant morphogenetic variations.

Our work sets the stage for further progress in understanding the unique mode of gastrulation in annual killifish. Further studies and the development of new tools in *Austrolebias* and other annual killifish species will help provide answers to the many questions raised by this study. For instance, in *Nothobranchius furzeri*, it is already possible to generate transgenic animals that express fluorescent proteins (Valenzano et al., 2011), and a genome sequence coupled with genome editing are available (Harel et al., 2015), all of which will aid in the cellular and molecular characterization of its development.

Experimental Procedures

Fish Maintenance and Husbandry

Adult wild-type *Austrolebias charrua* (Costa and Cheffe, 2001) and *Austrolebias bellottii* (Steindachner, 1881) were housed (one male and two females) in 40L glass aquaria. Aquaria contained reverse-osmosis water supplemented with salt (35g Microsalt [Brustmann] and 35g of Mineral Salt [Sera] per 10L water). The final water conditions were 200 μS of conductivity and pH 7.0 (adjusted with sodium bicarbonate). Biological filtration was provided, and plants were added to provide hide areas. Water temperature was maintained at 20 degC, and the photoperiod was set to 12 hr of light and 12 hr of dark. Fish were fed a varied diet primarily consisting of live food, which included adult brine shrimp (*Artemia salina*) and California blackworms, once or twice daily.

Egg Collection and Rearing of Killifish

Eggs were obtained through natural spawning. Commercial peat (previously boiled) served as the spawning media. The peat was placed in plastic containers, which allowed the fish to dig and spawn in it. Fertilized eggs were collected manually and cleaned by rolling them over wet filter paper with a brush. To produce a new generation of fish, the peat containing the eggs was partially dried to leave some moisture, placed in a zipped plastic bag, and left for at least three months at room temperature. Embryos were then placed in a petri dish containing embryo-rearing medium (ERM; 17.1mM NaCl, 402 μM KCl, 272 μM $CaCl_2$ 2[H_2O], 661 μM $MgSO_4$ 7[H_2O), pH 6.3], allowed to hatch, and then raised at 25 degC.

Embryo Staging and Imaging

DIC and confocal microscopy were used to stage *Austrolebias* embryos. For the DIC microscopy analysis, the embryos were mounted in a custom-made chamber that consisted of a tape pasted over a glass slide in which a rectangle was cut out in the center. The rectangular space was then filled with ERM, where the embryos were placed, and covered with a cover slip. This method allowed orienting the embryos by moving the cover slip. For confocal microscopy analysis, embryos at the one-cell stage were co-injected with mRNA encoding for *gap43-GFP* (membrane-tagged green fluorescent protein) and *H2B-RFP* (nuclear-localized red fluorescent protein). Injections were made using pulled borosilicate glass capillaries with an internal filament

(OD: 1mm, ID: 0.58mm; length: 10cm; Harvard Apparatus Ltd.). A puller (David Kopf Instruments, Model 740) was used to prepare the micropipettes using custom-defined settings. Embryos were raised at 25 degC in ERM until the stage of interest. Imaging was performed on Olympus Fluoview 1000 confocal and PerkinElmer Zeiss Axiovert 200 Spinning Disk microscopes using 10/NA0.3, 20/NA0.75, or 25W/NA0.8 objectives. Z-stacks were often captured at 1.5 μm intervals.

Image Processing

Deconvolution of confocal and spinning disc microscopy images was performed to improve signal/noise ratio and reduce blurring by Huygens Scripting Software (Scientific Volume Imaging, Hilversum, Netherlands). Image processing, z-stack projections, and 3D volume reconstruction were performed using Volocity (PerkinElmer), ImageJ 1.39t (Schneider et al., 2012), and SCIAN-Lab software (www.scian.cl) based on IDL 7.1.2 platform (Interactive Data Language, Exelis VIS, Boulder, Colorado).

Histological Sections

Austrolebias embryos at different stages of the reaggregation and axis formation process were cut in serial semithin sections using an embedding protocol for vibratome sections (Fernandez et al., 2006). The transverse thick sections, about 0.8 μm in thickness, were obtained with a Sorvall MT5000 Ultra Microtome. Approximately 600 sections were obtained from each embryo. Sections were stained with 1% Toluidine Blue in borate buffer and mounted with Entellan medium (Merck). Sections were microphotographed and the obtained images registered using ImageJ 1.39t (Schneider et al., 2012).

Lineage Tracing

Lineage-tracing analysis was conducted by injecting mRNA encoding for Kaede (Ando et al., 2002) into one-cell-stage embryos. After injection, embryos were incubated in ERM in the dark until the appropriate stage. The embryos with highest fluorescence intensity were selected and mounted in a camera with the target area oriented to the top. Selected cells were photoconverted with UV light for approximately one minute by reducing the diameter of the diaphragm or by using a pinhole in the epifluorescence light path. A record of the photoconversion position of target cells within the reaggregate at the stages of interest was made using an epifluorescence microscope.

Cloning of *Austrolebias* Genes

The *goosecoid* (*gsc*) and *brachyury* (*bra*) cDNA probes of *Austrolebias* were cloned by RT-PCR. Degenerate primers used were: *gsc*-F, 5′-TGCCIRCYGGIATGTTYWSIATHGA-3′; *gsc*-R, 5′-CAYTTIGCI CKICKRTTYTTRAACCA-3′; *bra*-F, 5′-TTCAARGAGCTIACCAAYG AGATGAT-3′; *bra*-R, 5′-TTGGCGAARGGGTTGTGYTTDATYTT-3′; where I represents Inosine, R (A/G), W (A/T), S (G/C), Y(C/T), K (G/T) and H (A/C/T). Sequences obtained from PCR products were compared to those of other vertebrates using BlastN (http://www.ncbi.nlm.nih.gov/BLAST/) to confirm amplification of the respective *Autrolebias* orthologs. ClustalW (http://www.ebi.ac.uk/tools/clustalw2/) was used for the alignment of sequences, and PROSITE (http://www.expasy.ch/prosite/) for the search of protein domains. Unrooted trees were constructed using the information obtained from ClustalW. The amino acid sequence of *Danio rerio Hox2.2* was used as an external reference gene for *gsc*, while *D. rerio tbx24* was used for *bra* (Supp. Fig. S1).

Whole-mount in situ Hybridization

Whole-mount in situ hybridization (WISH) and double-whole-mount in situ hybridization (D-WISH) were performed according to a protocol developed for Zebrafish embryos (Gamse et al., 2002), with the following modifications: The proteinase K treatment was eliminated, a rocker was not used, and antibodies were not pre-absorbed. Labeled antisense RNA probes for *Austrolebias bra* and *gsc* were synthesized using the specific partial coding sequences obtained from cloning. Histological sections of embryos subjected to WISH and D-WISH were performed as explained above using a thickness of sections 20 μm.

Acknowledgments

We thank Pablo Calviño and Roberto Petraccini for insight and animals, and Luis Cifuentes for dedicated animal care in our facility. We also thank María José Arezo, Nibia Berois, Soledad de La Piedra, Aldo Villalón, Miguel L. Allende, and Jason Podrabsky for fruitful discussions, valuable tips, and proofreading. Research in M.L.C.'s laboratory was supported by grants from the National Commission for Scientific and Technological Research (Ring Initiative ACT10769 and ACT47, FONDAP 15150012), the Millennium Science Initiative (P09-015-F), and the Howard Hughes Medical Institute (HHMI INTNL 55005940). S.H.'s laboratory was funded by FONDECYT 1151029, CONICYT PIA ACT1402, ICM P09-015-F, CORFO 16CTTS-66390, and DAAD (57220037 & 57168868). L.P. was funded by fellowships from FEBA, ICBM, DAAD (short-term fellowship), Mecesup (UCH0306), and FONDAP (15090007).

References

Ando R, Hama H, Yamamoto-Hino M, Mizuno H, Miyawaki A. 2002. An optical marker based on the UV-induced green-to-red photoconversion of a fluorescent protein. Proc Natl Acad Sci U S A 99:12651–12656.

Arezo MJ, Pereiro L, Berois N. 2005. Early development in the annual fish Cynolebias viarius. J Fish Biol 66:1357–1370.

Ballard WW, Dodes LM. 1968. The morphogenetic movements of the lower surface of the blastodisc in Salmonid embryos. J Exp Zool 168:76–84.

Bedzhov I, Zernicka-Goetz M. 2014. Self-organizing properties of mouse pluripotent cells initiate morphogenesis upon implantation. Cell 156:1032–1044.

Bertocchini F, Alev C, Nakaya Y, Sheng G. 2013. A little winning streak: the reptilian-eye view of gastrulation in birds. Dev Growth Differ 55:52–59.

Blum M, Gaunt SJ, Cho KW, Steinbeisser H, Blumberg B, Bittner D, De Robertis EM. 1992. Gastrulation in the mouse: the role of the homeobox gene goosecoid. Cell 69:1097–1106.

Carter CA, Wourms JP. 1991. Cell behavior during early development in the South American annual fishes of the genus Cynolebias. J Morphol 210:247–266.

Chuai M, Weijer CJ. 2008. The mechanisms underlying primitive streak formation in the chick embryo. Curr Top Dev Biol 81:135–156.

Coolen M, Nicolle D, Plouhinec JL, Gombault A, Sauka-Spengler T, Menuet A, Pieau C, Mazan S. 2008. Molecular characterization of the gastrula in the turtle Emys orbicularis: an evolutionary perspective on gastrulation. PLoS One 3:e2676.

Coolen M, Sauka-Spengler T, Nicolle D, Le-Mentec C, Lallemand Y, Da Silva C, Plouhinec JL, Robert B, Wincker P, Shi DL, Mazan

S. 2007. Evolution of axis specification mechanisms in jawed vertebrates: insights from a chondrichthyan. PLoS One 2:e374.
Costa WEJM. 1998. Phylogeny and classification of Rivulidae revisited: origin and evolution of annualism and miniaturization in rivulids fishes (Cyprinodontiformes: Aplocheiloidei). J Exp Zool A Comp Exp Biol 3:33–92.
Costa WJEM, Cheffe MM. 2001. Three new annual fishes of the genus Austrolebias from the Laguna dos Patos system, southern Brazil, and a redescription of A. adloffi (Ahl) (Ciprinodontiformes, Rivulidae). Com. Mus. Ciênc. PUCRS, Sér. Zool. Porto Alegre v. 14:179–200.
Elinson RP, del Pino E. 2011. Developmental diversity of amphibians. Wiley Interdiscip Rev Dev Biol 1:345–369.
Fernandez J, Valladares M, Fuentes R, Ubilla A. 2006. Reorganization of cytoplasm in the zebrafish oocyte and egg during early steps of ooplasmic segregation. Dev Dyn 235:656–671.
Gamse JT, Shen YC, Thisse C, Thisse B, Raymond PA, Halpern ME, Liang JO. 2002. Otx5 regulates genes that show circadian expression in the zebrafish pineal complex. Nat Genet 30: 117–121.
Godard BG, Mazan S. 2013. Early patterning in a chondrichthyan model, the small spotted dogfish: towards the gnathostome ancestral state. J Anat 222:56–66.
Harel I, Benayoun BA, Machado B, Singh PP, Hu CK, Pech MF, Valenzano DR, Zhang E, Sharp SC, Artandi SE, Brunet A. 2015. A platform for rapid exploration of aging and diseases in a naturally short-lived vertebrate. Cell 160:1013–1026.
Ho CY, Houart C, Wilson SW, Stainier DY. 1999. A role for the extraembryonic yolk syncytial layer in patterning the zebrafish embryo suggested by properties of the hex gene. Curr Biol 9: 1131–1134.
Kane D, Adams R. 2002. Life at the edge: epiboly and involution in the zebrafish. Results Probl Cell Differ 40:117–135.
Keller R, Davidson LA, Shook DR. 2003. How we are shaped: the biomechanics of gastrulation. Differentiation 71:171–205.
Kimmel CB, Ballard WW, Kimmel SR, Ullmann B, Schilling TF. 1995. Stages of embryonic development of the zebrafish. Dev Dyn 203:253–310.
Montero JA, Carvalho L, Wilsch-Brauninger M, Kilian B, Mustafa C, Heisenberg CP. 2005. Shield formation at the onset of zebrafish gastrulation. Development 132:1187–1198.
Nelson JS. 1984. Fishes of the world. New York: John Wiley & Sons. 523 p.
Royer LA, Lemon WC, Chhetri RK, Wan Y, Coleman M, Myers EW, Keller PJ. 2016. Adaptive light-sheet microscopy for long-term, high-resolution imaging in living organisms. Nat Biotechnol 34: 1267–1278.
Schneider CA, Rasband WS, Eliceiri KW. 2012. NIH Image to ImageJ: 25 years of image analysis. Nat Methods 9:671–675.
Schulte-Merker S, van Eeden FJ, Halpern ME, Kimmel CB, Nusslein-Volhard C. 1994. no tail (ntl) is the zebrafish homologue of the mouse T (Brachyury) gene. Development 120:1009–1015.
Solnica-Krezel L, Driever W. 2001. The role of the homeodomain protein Bozozok in zebrafish axis formation. Int J Dev Biol 45: 299–310.
Solnica-Krezel L, Sepich DS. 2012. Gastrulation: making and shaping germ layers. Annu Rev Cell Dev Biol 28:687–717.
Spemann H, Mangold H. 1924. Induction of embryonic primordial by implantation of organizers from a different species. Roux' Arch. Entw. Mech. 100:599–638.
Steindachner F. 1881. Beitrâge zur Kenntniss der Flussfische Sûdamerika's (III) und ichthyologische Beitrâge (XI). Anz Akad Wiss Wien:97–100.
Stern CD, Downs KM. 2012. The hypoblast (visceral endoderm): an evo-devo perspective. Development 139:1059–1069.
Tam PP, Loebel DA. 2007. Gene function in mouse embryogenesis: get set for gastrulation. Nat Rev Genet 8:368–381.
Technau U, Scholz CB. 2003. Origin and evolution of endoderm and mesoderm. Int J Dev Biol 47:531–539.
Valenzano DR, Sharp S, Brunet A. 2011. Transposon-Mediated Transgenesis in the Short-Lived African Killifish Nothobranchius furzeri, a Vertebrate Model for Aging. G3 (Bethesda) 1:531–538.
van den Brink SC, Baillie-Johnson P, Balayo T, Hadjantonakis AK, Nowotschin S, Turner DA, Martinez Arias A. 2014. Symmetry breaking, germ layer specification and axial organisation in aggregates of mouse embryonic stem cells. Development 141: 4231–4242.
Warga RM, Kane DA. 2003. One-eyed pinhead regulates cell motility independent of Squint/Cyclops signaling. Dev Biol 261:391–411.
Warga RM, Kimmel CB. 1990. Cell movements during epiboly and gastrulation in zebrafish. Development 108:569–580.
Warmflash A, Sorre B, Etoc F, Siggia ED, Brivanlou AH. 2014. A method to recapitulate early embryonic spatial patterning in human embryonic stem cells. Nat Methods 11:847–854.
Wei Y, Mikawa T. 2000. Formation of the avian primitive streak from spatially restricted blastoderm: evidence for polarized cell division in the elongating streak. Development 127:87–96.
Williams M, Burdsal C, Periasamy A, Lewandoski M, Sutherland A. 2012. Mouse primitive streak forms in situ by initiation of epithelial to mesenchymal transition without migration of a cell population. Dev Dyn 241:270–283.
Wourms JP. 1972a. The developmental biology of annual fishes. 3. Pre-embryonic and embryonic diapause of variable duration in the eggs of annual fishes. J Exp Zool 182:389–414.
Wourms JP. 1972b. Developmental biology of annual fishes. I. Stages in the normal development of Austrofundulus myersi Dahl. J Exp Zool 182:143–167.
Wourms JP. 1972c. The developmental biology of annual fishes. II. Naturally occurring dispersion and reaggregation of blastomers during the development of annual fish eggs. J Exp Zool 182: 169–200.
Yokoya S. 1966. Cell dissociation and reaggregation in early stage embryo of a teleost, *Oryzias latipes*. Sci Rep Tohoku Univ Ser 4 (Biol.) 32:229–236.